Pergamon

Int. J. Heat Mass Transfer. Vol. 38, No. 2, pp. 331–337, 1995

0017-9310/95 $9.50+0.00

0017-9310(94)00130-8

Numerical analysis of swirling non-reacting and reacting flows by the Reynolds stress differential method

MASAYA OHTSUKA

Energy Research Laboratory, Hitachi Ltd., 7-2-1 Omika-cho, Hitachi-shi, Ibaraki 319-12, Japan

(*Received* 4 *November* 1992 *and in final form* 7 *April* 1994)

Abstract—So *et al.*'s isothermal He–air mixing experiment and Wilhelmi's propane–air diffusion-controlled combustion experiment were analyzed with a differential Reynolds stress model. For both experiments, the IPC (isotropization of production and convection) model of Fu *et al.* for the rapid term improved the normal stress distribution in the large swirl velocity region and the Hanjalic and Launder model for the diffusion term improved the normal stress distribution near the centreline, in comparison with the IP (isotropization of production) model for the rapid term and the Daly and Harlow model for the diffusion term. For Wilhelmi's experiment, the IPC model and the Hanjalic and Launder model yielded improved mixture fraction distributions near the centreline. The intensity of axial and swirl velocities near the centreline was still underestimated, however, and the model requires further improvement.

INTRODUCTION

Numerical simulation is becoming a powerful aid in understanding combustion processes and designing combustion systems. One of the obstacles to predictive realism is the need to approximate turbulence transport in a combustor by using turbulence models. Swirl is a flow frequently induced in combustors, where it plays important roles in mixing fuel and oxide, and stabilizing the flame. In swirling flow, turbulence can be highly non-isotropic because of the action of the flow curvature and centrifugal acceleration. Swirling reactive flow becomes more complicated due to variable density and chemical reactions.

A strongly swirling, confined, constant-density flow was measured by So *et al.* [1] and was calculated using the standard k–ε eddy viscosity model and the DRSM (differential Reynolds stress model) by Hogg and Leschziner [2]. In the standard DRSM, the IP (isotropization of production) model for the rapid term, the Rotta model for the return-to-isotropy term and Daly and Harlow's model for the diffusion term are used. The k–ε model was founded to given an excessively large turbulence diffusion, but the DRSM successfully represented the lower level of shear stress, and predictions of velocity and turbulence fields agree well with the experiment. Fu *et al.* [3] applied the DRSM to the swirling, isothermal, constant-density flow, measured by Sislian and Cusworth [4]. The modelling framework featured the IPC (isotropization of production and convection) model, which includes the convection effect in the rapid term to achieve material invariance in the co-ordinate system. The study demonstrated that the inclusion of the convection effect in the rapid term results in a remarkable improvement in the predicted turbulence–stress fields.

Hogg and Leschziner [5] applied the density-weighted DRSM to a swirling confined flow measured by So *et al.* [2], which consisted of an outer strongly swirling annular air stream and an inner non-swirling helium jet. This model included an additional pressure-driven generation term due to the density variation in the standard DRSM and was found to simulate correctly the strong suppression of radial turbulent exchange of momentum and mass. Radial mass mixing, however, was still overpredicted.

Using the same revised model, Hogg and Leschziner [6] also calculated the strongly-swirling reacting flow measured by Wilhelmi [7]. They included pdf closure for the combustion model, which assumed fast chemical reactions and an equilibrium state for the burned gases. The calculated results indicated that the second-moment closure yielded no decisive advantage over the eddy viscosity approach. With both models, there were large discrepancies between prediction and experiment, especially with regard to the temperature and the mixture fraction around the centreline. Hogg and Leschziner concluded that defects arose principally from the combustion model and uncertainties in the boundary conditions.

There is no doubt, however, that turbulence model defects played a contributory role. In particular, the pressure redistribution term, diffusion term and dissipation term of turbulent stresses and scalar fluxes need to be better modelled. Fu *et al.* [3] introduced the IPC model for the rapid term for swirling constant-density flow, but the model has never been evaluated for swirling variable-density flow. Hogg and Leschziner [5] noted that the erroneous representation of the turbulent scalar flux was especially important with respect to the agreement with the experimental mass fraction distribution of So *et al.* [1]. The IPC model

NOMENCLATURE

C	turbulence constant or convection term
D	diffusion term or diameter of Wilhelmi's combustor [m]
F	mixing fraction
f	fluctuation of F
G	density-related production term
g	turbulent scalar intensity, f^2
k	turbulence energy [m^{-2} s^{-2}]
P	velocity-related production or pressure [Pa]
R	radius of test section [m]
r	radius [m]
T	temperature [K]
U	velocity or axial velocity
u	fluctuation of U [m s^{-1}]
V	radial velocity [m s^{-1}]
v	fluctuation of V [m s^{-1}]
W	swirl velocity [m s^{-1}]
w	fluctuation of W [m s^{-1}]
X	position or axial distance [m].

Greek symbols

ε	dissipation of k [m^{-2} s^{-3}]
ρ	density [kg m^{-3}].

Indices

$ijkl$	index of direction
$\hat{}$	time average
$\sim$	density average.

of turbulent stresses may indirectly affect the turbulent scalar flux field. Moreover, the modelling of diffusion can significantly affect the turbulent mixing of velocity and mass. The dissipation term of the turbulent energy and scalar variance also introduces ambiguity into the model and affects not only the turbulent energy and turbulent scalar intensity, but also the mixing time ratio of the velocity and mass.

In this study, the earlier DRSM [5, 6] was modified in an effort to improve the accuracy for swirling, variable-density flow. Specifically, the rapid pressure–strain term and the diffusion term of the DRSM were altered. So *et al.*'s [1] isothermal experiment and Wilhelmi's [7] reacting experiment were analyzed, and the present computational results were compared with the solutions obtained by Hogg and Leschziner's model [5, 6].

MATHEMATICAL DESCRIPTION

The analytical model was based on Hogg and Leschziner's model [5, 6]. Basic transport equations were conservation equations of mass, momentum, mixture fraction, turbulent stress, turbulent energy dissipation, turbulent scalar intensity and turbulent scalar flux. The transported quantities are the following from density-weighted (Favre) averaging:

$$\tilde{\psi} = \frac{\overline{\rho\psi}}{\bar{\rho}}. \tag{1}$$

The transport equations then arise as follows:

$$\frac{1}{r}\frac{\partial r\bar{\rho}\tilde{U}_i\tilde{\psi}}{\partial x_i} = S_\psi \tag{2}$$

$$\frac{1}{r}\frac{\partial r\bar{\rho}\tilde{U}_i\widetilde{u_iu_j}}{\partial x_i} = D_{ij}+P_{ij}+G_{ij}+\phi_{ij}-\frac{2}{3}\bar{\rho}\delta_{ij}\tilde{\varepsilon} \tag{3}$$

$$\frac{1}{r}\frac{\partial r\bar{\rho}\tilde{U}_i\tilde{\varepsilon}}{\partial x_i} = D_\varepsilon+\frac{\tilde{\varepsilon}}{\tilde{k}}(C_{\varepsilon1}P_{kk}+C_{\varepsilon2}\bar{\rho}\tilde{\varepsilon}+C_{\varepsilon3}G_{kk}) \tag{4}$$

Table 1. Sources of transport equations (2)

ψ	$S\psi$
$\tilde{U}$	$-\partial\bar{P}/\partial x-\partial\bar{\rho}\widetilde{u^2}/\partial x-\partial(r\bar{\rho}\widetilde{uw})/r\,\partial r$
$\tilde{V}$	$-\partial\bar{P}/\partial r+\bar{\rho}(\widetilde{W^2}+\widetilde{w^2})/r-\partial(r\bar{\rho}\widetilde{v^2})/r\,\partial r$ $-\partial(\bar{\rho}\widetilde{uv})/\partial x$
$r\tilde{W}$	$-\partial(\bar{\rho}\widetilde{uw})/r\,\partial x-r\,\partial(\bar{\rho}\widetilde{vw})/\partial r-2\bar{\rho}\widetilde{vw}$
$\tilde{F}$	$-\partial(\bar{\rho}\widetilde{uf})/\partial x-\partial(\bar{\rho}\widetilde{vf})/r\,\partial r$

$$\frac{1}{r}\frac{\partial r\bar{\rho}\tilde{U}_i\tilde{g}}{\partial x_i} = D_g-2\bar{\rho}\widetilde{u_if}\frac{\partial F}{\partial x_i}-2C_d\bar{\rho}\tilde{g}\frac{\tilde{\varepsilon}}{\tilde{k}} \tag{5}$$

$$\frac{1}{r}\frac{\partial r\bar{\rho}\tilde{U}_i\widetilde{u_if}}{\partial x_i} = D_{if}+P_{if}+G_{if}+\phi_{if}. \tag{6}$$

ψ and $S\psi$ are shown in Table 1. D, P, G and Φ are the diffusion, strain production, production due to density variation, and pressure redistribution terms, respectively. The indices ij and if represent the terms $\widetilde{u_iu_i}$ and $\widetilde{U_if}$, respectively. The additional terms produced by the transformation from the Cartesian to the cylindrical coordinates system are shown in Tables 2 and 3. The return-to-isotropy term in ϕ_{ij} was modelled according to Rotta's proposal [8], and the two wall-correction terms, corresponding to the stress and production isotropization in ϕ_{ij}, proposed by Shir [9] and Gibson and Launder [10] were adopted.

The IP model of Naot *et al.* [11] has been generally used for the rapid term in ϕ_{ij} and has been retained herein. Convection of the non-isotropic turbulence, however, is important for swirling flow modelling. The IPC model of Fu *et al.* [3], which includes the convection effect, was introduced for both of the rapid terms, $\phi_{ij,2}$ and $\phi_{if,2}$:

Table 2. Additional terms of transport equations (3) for convection and production

$\widetilde{u_iu_j}$	Convection	Production
$\widetilde{u^2}$	—	—
$\widetilde{v^2}$	$+2\bar{\rho}\widetilde{uw}\tilde{W}/r$	$+2\bar{\rho}\widetilde{uw}\tilde{W}/r$
$\widetilde{w^2}$	$-2\bar{\rho}\widetilde{vw}\tilde{W}/r$	$-2\bar{\rho}\widetilde{w^2}\tilde{V}/r$
$\widetilde{uv}$	$+\bar{\rho}\widetilde{uw}\tilde{W}/r$	$+\bar{\rho}\widetilde{uw}\tilde{W}/r$
$\widetilde{vw}$	$-\bar{\rho}(\widetilde{v^2}-\widetilde{w^2})\tilde{W}/r$	$-\bar{\rho}\widetilde{uw}\tilde{V}/r+\bar{\rho}\widetilde{w^2}\tilde{W}/r$
$\widetilde{uw}$	$-\bar{\rho}\widetilde{uv}\tilde{W}/r$	$-\bar{\rho}\widetilde{uw}\tilde{V}/r$

Table 3. Additional terms of transport equations (6) for convection and production

$\widetilde{u_if}$	Convection	Production
$\widetilde{uf}$	—	—
$\widetilde{vf}$	$+\bar{\rho}\widetilde{wf}\tilde{W}/r$	$+\bar{\rho}\widetilde{wf}\tilde{W}/r$
$\widetilde{wf}$	$+\bar{\rho}\widetilde{vf}\tilde{W}/r$	$+\bar{\rho}\widetilde{wf}\tilde{V}/r$

IP model

$$\phi_{ij,2} = -C_2(P_{ij}-\tfrac{1}{3}\delta_{ij}P_{kk}) \tag{7}$$

$$\phi_{if,2} = -C_2'P_{ic} \tag{8}$$

IPC model

$$\phi_{ij,2} = -C_2(P_{ij}+C_{ij}-\tfrac{1}{3}\delta_{ij}P_{kk}-\tfrac{1}{3}\delta_{ij}C_{kk}) \tag{9}$$

$$\phi_{if,2} = -C_2'(P_{ic}+C_{if}). \tag{10}$$

P_{ic} is a part of P_{if} including the velocity gradient and the C in the parentheses represents the convection term.

The Daly and Harlow model [12] is generally used for the diffusion term of the turbulent stress. This model, written for simplicity in Cartesian tensor notation, is as follows:

$$D_{ij} = \frac{\partial}{\partial x_l}\left(C_k\bar{\rho}\frac{\tilde{k}}{\tilde{\varepsilon}}\widetilde{u_ku_l}\frac{\partial\widetilde{u_iu_j}}{\partial x_l}\right). \tag{11}$$

This model is not invariant for interchanging the indices ijk and does not satisfy symmetry of diffusion terms for $i \neq j \neq k$. In a cylindrical coordinate system, a noticeable error may occur around the centreline which is a singular point. Therefore, the following model of Hanjalic and Launder [13] was used instead:

$$D_{ij} = \frac{\partial}{\partial x_l}\left(C_k'\bar{\rho}\frac{\tilde{k}}{\tilde{\varepsilon}}\widetilde{u_ku_l}\frac{\partial\widetilde{u_iu_j}}{\partial x_k}\right) + \frac{\partial}{\partial x_l}\left(C_k'\bar{\rho}\frac{\tilde{k}}{\tilde{\varepsilon}}\widetilde{u_iu_l}\frac{\partial\widetilde{u_ku_j}}{\partial x_k}\right) + \frac{\partial}{\partial x_l}\left(C_k'\bar{\rho}\frac{\tilde{k}}{\tilde{\varepsilon}}\widetilde{u_ju_l}\frac{\partial\widetilde{u_ku_i}}{\partial x_k}\right). \tag{12}$$

The expression for D_{ij} in cylindrical coordinates can be found in ref. [5] for the Daly and Harlow model and in Appendix A of the present paper for the Hanjalic and Launder model. Turbulence model constants are listed in Table 4.

Table 4. Turbulence model constants

C_2	C_2'	C_k	C_k'	$C_{\varepsilon1}$	$C_{\varepsilon2}$	$C_{\varepsilon3}$	C_d
0.6	0.5	0.22	0.11	1.44	1.92	0.95	0.5

The effect of turbulence on temperature and density can be introduced by using the pdf. When fast chemical reactions are assumed for the combustion calculation, temperature and density can be given as unique functions of the mixture fraction. The density-weighted average for the temperature, $\tilde{T}$, and the time average for the density, $\bar{\rho}$, are then as follows:

$$\tilde{T} = \int_0^1 T(F)P(F)\,\mathrm{d}F \tag{13}$$

$$\frac{1}{\bar{\rho}} = \int_0^1 \frac{P(F)}{\rho(F)}\,\mathrm{d}F \tag{14}$$

where the following so-called β-pdf was assumed:

$$P(F) = \frac{F^{a-1}(1-F)^{b-1}}{\displaystyle\int_0^1 F^{a-1}(1-F)^{b-1}\,\mathrm{d}F} \tag{15}$$

$$a = \left\{\frac{(1-F)F}{\tilde{g}} - 1.0\right\}F \tag{16}$$

$$b = \left\{\frac{(1-F)F}{\tilde{g}} - 1.0\right\}(1-F). \tag{17}$$

In this study, the chemical reaction was assumed to be a one-step irreversible process with an infinite reaction rate, and only the chemical elements related to the one-step reaction were considered.

The discretization method was based on the finite-volume approach. The solution alogorithm was iterative in nature and the SIMPLE method was adopted in conjunction with the tri-diagonal matrix algorithms for solving the linearized systems of the finite-volume equation. The QUICK method was used for the convection terms of the momentum, and the power law discretization scheme was used for the convection terms of the other quantities. The diffusion terms were discretized by the central difference method. The numerical framework was basically Hogg and Leschziner's code [5, 6].

RESULTS

Isothermal calculation

So *et al.*'s [1] experiment was analysed. The configuration is shown in Fig. 1. An He–air jet (volume ratio = 9) was injected into a cylindrical vessel along the centreline and swirling air was introduced around the central jet. The swirl number at the inlet was 2.25.

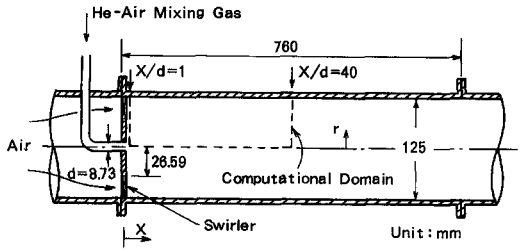

Fig. 1. Computation flow configuration (So *et al.*'s [1] experiment).

A two-dimensional cylindrical polar coordinate system was used. Inlet conditions were prescribed at $X/d = 5$ because no experimental data were available further upstream. X is the distance from the inlet and d is the diameter of the He–air jet pipe. Transported quantities were prescribed at the inlet plane and radial gradients of the quantities were nullified at the centreline. At the wall, shear stresses were evaluated via log-law relations. At the outlet, axial velocity was prescribed by reference to the experimental distribution while all other normal gradients to the boundary were set to zero.

Figure 2 shows the radial distribution of velocity, turbulent normal stress and mass fraction at $X/d = 10$ and 40. Here, the standard model was that of Hogg and Leschziner [5], the IPC model was the standard Hogg and Leschziner variant except for the rapid term of the IPC model, and the Hanjalic and Launder model was the same as the standard Hogg and Leschziner version, except for the diffusion term [12].

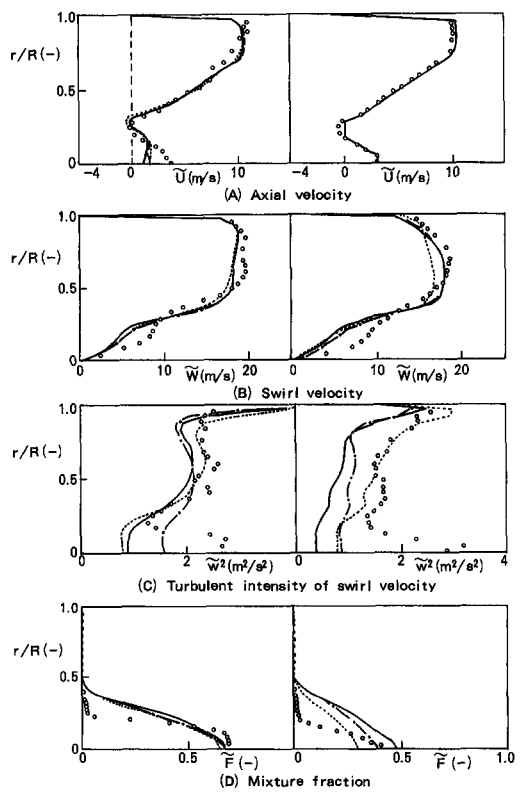

Fig. 2. Computed radial profiles of So *et al.*'s [1] experiment [left: $X/d = 10$, right: $X/d = 40$; experimental data (○), standard model (———), IPC model (– – – –), Hanjalic and Launder model (— · — · —)].

As seen from Fig. 2, the light He–air jet along the centreline remains separated from the surrounding air due to centripetal accelerations. The distribution of calculated quantities at $X/d = 40$ is almost the same as that at $X/d = 10$. Variations in the models did not significantly change the velocity distribution. The Hanjalic and Launder model gave a slightly better fit for the velocity distribution near the centreline. An increase in circumferential normal stress was returned in the swirling outer air flow by the IPC model and at the centre by the Hanjalic and Launder diffusion model. Overall, the IPC model gave a better representation of the swirling flow air in outer radial locations.

The additional term $-2\bar{\rho}\widetilde{vw}\widetilde{W}/r$ in the convection of $\widetilde{w^2}$ decreased $\widetilde{w^2}$ because $\widetilde{vw}$ is positive. The IPC model is able to account for this effect thorough the rapid term because the convection effect could be taken into account by the rapid term and enlarged $\widetilde{w^2}$ in the swirling flow. On the other hand, the Hanjalic and Launder diffusion model changed the value of $\widetilde{w^2}$ at the centre, where the transformation variation from the Cartesian coordinate to cylindrical coordinate accumulated. The large peak for $\widetilde{w^2}$ near the centreline could not be reproduced by any of the models, however.

Discrepancies between computation and experiment mainly occur near the centreline, where calculated velocities are smaller than experimental values. The reduction in the axial velocity near the centreline at $X/d = 10$ is related to the reduction in the swirl velocity. The reduction in the swirl velocity increases the pressure along the centreline and the light He–air mixing gas consequently tends to decelerate. The reduction in the swirl velocity is related to the shear stress $\widetilde{vw}$ which was the most influential component of the shear stress in relation to the swirl velocity $\widetilde{W}$.

Figure 3 shows the radial distribution of $\widetilde{vw}$ with the Hogg and Leschziner model at $X/d = 10$. The shear stress $\widetilde{vw}$ had its local maximum in the mixing layer of the He–air jet and surrounding air. The source

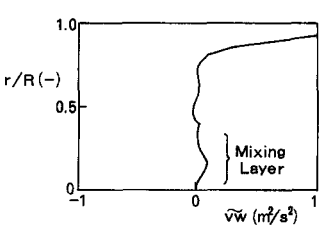

Fig. 3. Radial distribution of $\widetilde{vw}$ at $X/d = 10$ (standard model).

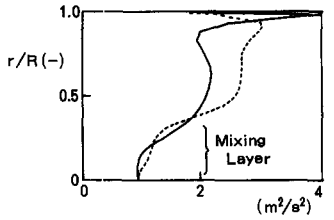

Fig. 4. Radial distribution of $\widetilde{v^2}$ and $\widetilde{w^2}$ at $X/d = 10$ (standard model).

of the swirl velocity $\tilde{W}$ is proportional to $-\widetilde{vw}$ near the centreline and increasing $\widetilde{vw}$ decreases $\tilde{W}$. Figure 4 shows the radial distribution of $\widetilde{v^2}$ and $\widetilde{w^2}$ at $X/d = 10$. The difference between $\widetilde{v^2}$ and $\widetilde{w^2}$ increases where $\widetilde{vw}$ had the local maximum, which is caused by the generation term of $\widetilde{vw}$ being proportional to the difference between the radial normal stress $\widetilde{v^2}$ and the swirl normal stress $\widetilde{w^2}$ near the centreline. Therefore, the accuracy of $\widetilde{v^2}$ and $\widetilde{w^2}$ affects the velocity distribution through $\widetilde{vw}$ and should be improved to improve the accuracy of the swirl and axial velocity near the centreline.

As shown in Fig. 2, the calculated mixture fraction is more diffusive than is indicated by the experimental data. The radial mixture fraction distribution arising from the IPC and Hanjalic and Launder models were diffusive in comparison with the standard model. Radial diffusion of the mixture fraction is characterized by the radial turbulent scalar flux $\widetilde{vf}$. There are no experimental data for $\widetilde{vf}$ but the intensity of the turbulent mixture fraction $\tilde{g}$ was measured. Figure 5 shows the radial distribution of $\tilde{g}$ at $X/d = 10$. The intensity of the turbulent mixture fraction $\tilde{g}$ was included in the pressure-related generation term G_{ij}, which is the product of g and the pressure gradient. The IPC and Hanjalic and Launder models increase the absolute value of $\tilde{g}$ and give a better agreement with the experiment. Increasing $\tilde{g}$ should make $\widetilde{vf}$ decrease; the improvement of $\tilde{g}$ cannot, therefore, contribute to the improvement of $\tilde{F}$ diffusion. The excess diffusion by the IPC model or the Hanjalic and Launder model was due to the increase in the turbulent normal stress and $\tilde{g}$. An accurate prediction of turbulent normal stress must therefore be achieved to improve the mixture fraction profile.

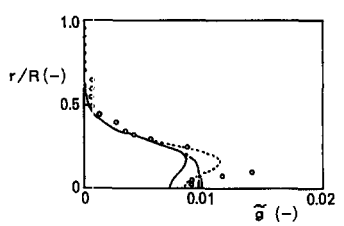

Fig. 5. Radial distribution of turbulent scalar intensity at $X/d = 10$ [experimental data (○), standard model (——), IPC model (– – –), Hanjalic and Launder model (— · — ·)].

Combustion calculation

Wilhelmi's experiment was analysed using the configuration shown in Fig. 6. The calculation domain was two-dimensional, in terms of cylindrical polar coordinates. The fuel was propane and the swirl number due to swirling air was 0.78 at the inlet. Boundary conditions were treated in a manner similar to those in the calculation of So *et al.*'s experiment except at the inlet and outlet. The inlet was set at $X = 0$. The axial velocity was set to be gradient-free at the outlet because there was no inflow at the outlet in Wilhelmi's experiment.

Figure 7 shows the distributions of the velocity, temperature, fuel mixture fraction and turbulent normal stresses at $X/D = 0.1$ and 1.0. There is a recirculation zone near the centreline at $X/D = 0.1$. The experimental results show that a hot region is formed around the centreline, but the calculated temperature is substantially lower than the experimental one. Correspondingly, the calculated mixture fraction was higher than the experimental value around the centreline. Unburned propane was present around the centreline and hot products, formed downstream, are not carried upstream because of a weak recirculation zone. The calculated results obtained with the Hanjalic and Launder model are better than the others in relation to the temperature and mixture fraction around the centreline.

At $X/D = 1.0$, the discrepancies between the numerical and experimental results of the mixture fraction and temperature could be remarkably decreased by the use of the IPC model or the Hanjalic and Launder model. Figure 8 shows the distributions of the calculated radial turbulent mass flux $\widetilde{vf}$, which governs fuel and air mixing in the radial direction. Figure 9 shows the radial turbulent normal stress $\widetilde{v^2}$, which is included in the production term of $\widetilde{vf}$. The increase in the peak for $\widetilde{vf}$ arising with the IPC model near $X/D = 0.5$ is not due to the production term, but the pressure redistribution term of $\widetilde{vf}$, because $\widetilde{v^2}$ from the IPC model is almost the same as that from the IP model. On the other hand, for the Hanjalic and Launder model, $\widetilde{v^2}$ is higher, which affects $\widetilde{vf}$ through its production term near the centreline. The flux $\widetilde{vf}$ of the IPC model or the Hanjalic and Launder model increases for $X/D \sim 0.38$ and 0.26, respectively, in comparison with the standard model, which meant decreased discrepancies between the experimental and

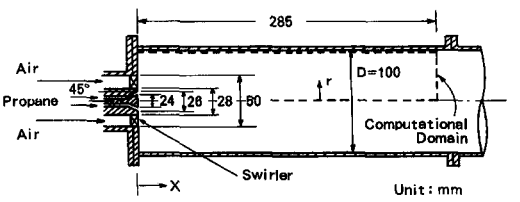

Fig. 6. Computation flow configuration (Wilhelmi's [7] experiment).

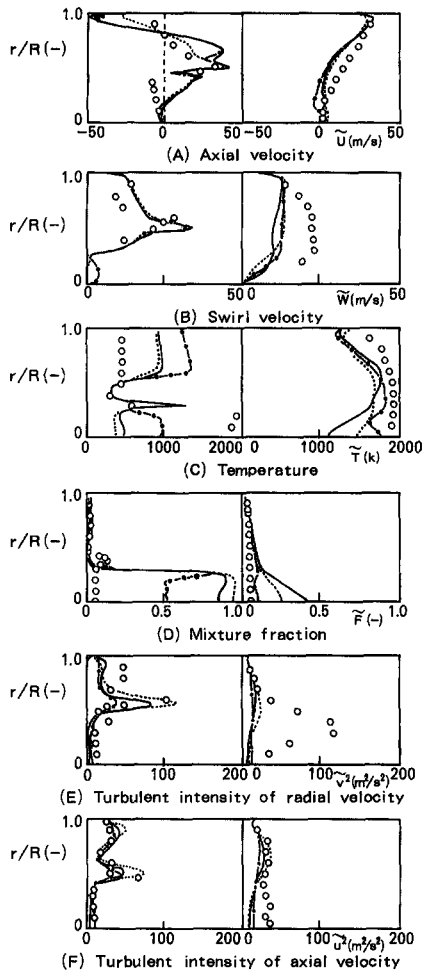

Fig. 7. Computed radial profiles of Wilhelmi's [7] experiment [left: $X/d = 0.1$, right: $X/d = 1.0$; experimental data (○), standard model (——), IPC model (– – –), Hanjalic and Launder model (— · —)].

numerical results for the mixture fraction and temperature around the centreline.

The calculated swirl velocity was smaller than the experimental value near the centreline at $X/D = 1.0$. The reduction in the swirl velocity is related to the shear stress $\widetilde{vw}$, as was the case in So *et al.*'s experiment. In Wilhelmi's experiment, an additional thermal effect occurs. At $X/D = 1.0$, the absolute numerical value of the temperature is lower than the experimental value, which causes an increase in density and a decrease in swirl velocity. The calculated low temperature was caused by the heat loss from the cooled side wall and/or a lower reaction rate for the fuel. Therefore, further agreement for the swirl velocity is likely to be achieved only by improving the combustion model.

In the experiment, a strong anisotropic turbulence occurred at $X/D = 1.0$ and the radial turbulent normal stress $\widetilde{v^2}$ was larger than the other normal stress components. The anisotropy might be caused by the large-scale periodic motion of fluid or precession around the centerline due to asymmetry of the test conditions or instability. The computational model cannot simulate such a motion and computational results could not reproduce the strong anisotropic turbulence. However, the IPC model improved the normal stress distribution where the swirl velocity was large and the Hanjalic and Launder model improved the normal stress distribution near the centreline.

CONCLUSIONS

So *et al.*'s isothermal He–air mixing experiment and Wilhelmi's propane–air diffusion-controlled combustion experiment were analysed with a DRSM. The standard model, containing the IP model for the rapid term, and the Daly and Harlow model for diffusion were replaced by the IPC model and the Hanjalic and Launder model, respectively. The following major conclusions arose from the study:

(1) For both experiments, the IPC model gave a better agreement for the normal stress distribution where the swirl velocity was large, and the Hanjalic and Launder model yielded an improvement for the normal stress distribution near the centreline.
(2) For Wilhelmi's experiment, the IPC and Hanjalic and Launder models yielded improved mixture fraction distributions near the centreline.
(3) The intensity of the axial and swirl velocities near the centreline was still underestimated and the model requires further improvement.

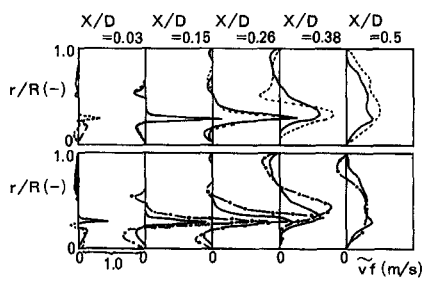

Fig. 8. Radial profile of $\widetilde{vf}$ [standard model (——), IPC model (– – –), Hanjalic and Launder model (—·)].

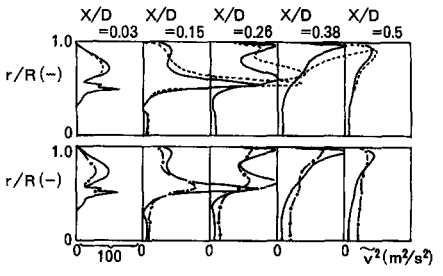

Fig. 9. Radial profile of $\widetilde{v^2}$ [standard model (——), IPC model (– – –), Hanjalic and Launder model (—·)].

Acknowledgements—The author is greatly indebted to Prof. M. A. Leschziner (University of Manchester Institute of Technology) and Dr S. I. Hogg (Oxford University) for many variable discussions and computational support.

REFERENCES

1. R. M. So, S. A. Ahmed and H. C. Mongia, An experimental investigation of gas jets in confined swirling air flow, NASA CR3892 (1984).
2. S. I. Hogg and M. A. Leschziner, Computation of highly swirling confined flow with a Reynolds stress turbulence model, *AIAA J.* **27**, 57–63 (1989).
3. S. Fu, B. E. Launder and M. A. Leschziner, Modelling strongly recirculating jet flow with Reynolds-stress transport closures, *Proceedings of the 6th Symposium on Turbulent Shear Flows*, Toulouse, pp. 17.6.1–17.6.6 (1987).
4. J. P. Sislian and R. A. Cusworth, Laser Doppler velocimetry measurements in a free isothermal swirling jet, Report No. 281, CN ISSN.0082-5255, University of Toronto Institute of Applied Science (1984).
5. S. I. Hogg and M. A. Leschziner, Second moment closure calculation of strongly swirling confined flow with large density gradients, *Int. J. Heat Fluid Flow* **10**, 16–27 (1989).
6. S. I. Hogg and M. A. Leschziner, Computation of strongly-swirling reacting flow in a model combustor with second-moment closure, *Proceedings of the 7th Symposium on Turbulent Shear Flows*, Stanford University, pp. 23.5.1–23.5.6 (1989).
7. J. Wilhelmi, Axisymmetric swirl stabilized combustion, PhD thesis, University of London (1984).
8. J. C. Rotta, *Z. Phys.* **129** 547 (1951).
9. C. C. Shir, A preliminary numerical study of atmospheric turbulent flows in the idealised planetary boundary layer, *J. Atmos. Sci.* **30**, 1327 (1973).
10. M. M. Gibson and B. E. Launder, Ground effects on pressure fluctuations in the atmospheric boundary layer, *J. Fluid Mech.* **86**, 491 (1978).
11. D. Naot, A. Shavit and M. Wolfshtein, Two point correlation model and the redistribution of Reynolds stresses, *Phys. Fluids* **16**, 738 (1973).
12. B. J. Daly and F. H. Harlow, Transport equations in turbulence, *Phys. Fluids* **13**, 2634 (1970).
13. K. Hanjalic and B. E. Launder, A Reynolds stress model of turbulence and its application to thin shear flows, *J. Fluid Mech.* **52**, 609 (1972).

APPENDIX

The diffusion term D_{ij} of the turbulent stress can be written in tensor form as follows:

$$D^{ij} = A^{ijk}_{|k} \tag{A1}$$

where D^{ij} is the covariant tensor of D_{ij}. The covariant tensors of D^{ij} and A^{ijk} by the Hanjalic and Launder model are shown in Tables A1 and A2.

Table A1. Covariant tensors of diffusion term D^{ij}†

$\widetilde{u_i u_j}$	D^{ij}
$\widetilde{v^2}$	$-1/r\cdot\partial(rA^{111})/\partial r-\partial A^{113}/\partial x+2rA^{122}$
$\widetilde{w^2}$	$-1/r\cdot\partial(rA^{122})/\partial r-\partial A^{223}/\partial x-2A^{122}/r$
$\widetilde{u^2}$	$-1/r\cdot\partial(rA^{133})/\partial r-\partial A^{333}/\partial x$
$\widetilde{uv}$	$-1/r\cdot\partial(rA^{113})/\partial r-\partial A^{133}/\partial x+rA^{223}$
$\widetilde{uw}$	$-1/r\cdot\partial(rA^{123})/\partial r-\partial A^{223}/\partial x-2A^{123}/r$
$\widetilde{vw}$	$-1/r\cdot\partial(rA^{112})/\partial r-\partial A^{123}/\partial x-2A^{112}/r+rA^{222}$

† $(u_1, u_2, u_3) = (v, w, u)$.

Table A2. Covariant tensors of A^{ijk}

A^{111}	$-3C_k/2\cdot\tilde{k}/\tilde{\varepsilon}\cdot(\widetilde{v^2}\,\partial\widetilde{v^2}/\partial r+\widetilde{uv}\,\partial\widetilde{v^2}/\partial x-2\widetilde{vw^2}/r)$
A^{222}	$-3C_k/2\cdot\tilde{k}/\tilde{\varepsilon}/r^3\cdot(\widetilde{vw}\,\partial\widetilde{w^2}/\partial r+\widetilde{uw}\,\partial\widetilde{w^2}/\partial x+2\widetilde{w^2}\cdot\widetilde{vw}/r)$
A^{333}	$-3C_k/2\cdot\tilde{k}/\tilde{\varepsilon}\cdot(\widetilde{uv}\,\partial\widetilde{u^2}/\partial r+\widetilde{u^2}\,\partial\widetilde{v^2}/\partial x)$
A^{112}	$-C_k/2\cdot\tilde{k}/\tilde{\varepsilon}/r\cdot\{2\widetilde{v^2}\,\partial\widetilde{vw}/\partial r+2\widetilde{uv}\,\partial\widetilde{vw}/\partial x+\widetilde{vw}\,\partial v^2/\partial r+\widetilde{uw}\,\partial\widetilde{v^2}/\partial x+2\widetilde{vw}(\widetilde{v^2}-2\widetilde{w^2})/r\}$
A^{113}	$-C_k/2\cdot\tilde{k}/\tilde{\varepsilon}\cdot(2\widetilde{v^2}\,\partial\widetilde{uv}/\partial r+2\widetilde{uv}\,\partial\widetilde{uv}/\partial x+\widetilde{uv}\,\partial\widetilde{v^2}/\partial r+\widetilde{u^2}\,\partial\widetilde{v^2}/\partial x-4\widetilde{vw}\cdot\widetilde{vw}/r)$
A^{122}	$-C_k/2\cdot\tilde{k}/\tilde{\varepsilon}/r^2\cdot\{2\widetilde{vw}\,\partial\widetilde{vw}/\partial r+2\widetilde{uw}\,\partial\widetilde{vw}/\partial x+\widetilde{v^2}\,\partial\widetilde{w^2}/\partial r+\widetilde{uv}\,\partial\widetilde{w^2}/\partial x+2\widetilde{w^2}(\widetilde{v^2}-\widetilde{w^2})/r+2\widetilde{vw^2}/r\}$
A^{133}	$-C_k/2\cdot\tilde{k}/\tilde{\varepsilon}\cdot(2\widetilde{uv}\,\partial\widetilde{uv}/\partial r+2\widetilde{u^2}\,\partial\widetilde{uv}/\partial x+\widetilde{v^2}\,\partial\widetilde{u^2}/\partial r+\widetilde{uv}\,\partial\widetilde{u^2}/\partial x-2\widetilde{uw^2}/r)$
A^{223}	$-C_k/2\cdot\tilde{k}/\tilde{\varepsilon}/r^2\cdot\{2\widetilde{vw}\,\partial\widetilde{uw}/\partial r+2\widetilde{uw}\,\partial\widetilde{uw}/\partial x+\widetilde{uv}\,\partial\widetilde{w^2}/\partial r+\widetilde{u^2}\,\partial\widetilde{w^2}/\partial x+2(\widetilde{w^2}\cdot\widetilde{uv}+\widetilde{uw}\cdot\widetilde{vw})/r\}$
A^{233}	$-C_k/2\cdot\tilde{k}/\tilde{\varepsilon}/r\cdot(2\widetilde{uv}\,\partial\widetilde{uw}/\partial r+2\widetilde{u^2}\,\partial\widetilde{uw}/\partial x+\widetilde{vw}\,\partial\widetilde{u^2}/\partial r+\widetilde{uw}\,\partial\widetilde{u^2}/\partial x+2\widetilde{uw}\cdot\widetilde{uv}/r)$
A^{123}	$-C_k/2\cdot\tilde{k}/\tilde{\varepsilon}/r\cdot\{\widetilde{v^2}\,\partial\widetilde{uw}/\partial r+\widetilde{uv}\,\partial\widetilde{uw}/\partial x+\widetilde{vw}\,\partial\widetilde{uv}/\partial r+\widetilde{uv}\,\partial\widetilde{vw}/\partial r+\widetilde{uv}\,\partial\widetilde{vw}/\partial r+\widetilde{u^2}\,\partial\widetilde{vw}/\partial x+\widetilde{vw}\cdot\widetilde{uv}/r+\widetilde{uw}(\widetilde{v^2}-2\widetilde{w^2})/r\}$